

Fine-Tuning the Energy Levels of a Nonfullerene Small-Molecule Acceptor to Achieve a High Short-Circuit Current and a Power Conversion Efficiency over 12% in Organic Solar Cells

Bin Kan, Jiangbin Zhang, Feng Liu, Xiangjian Wan, Chenxi Li, Xin Ke, Yunchuang Wang, Huanran Feng, Yamin Zhang, Guankui Long, Richard H. Friend, Artem A. Bakulin,* and Yongsheng Chen*

Organic solar cell optimization requires careful balancing of current–voltage output of the materials system. Here, such optimization using ultrafast spectroscopy as a tool to optimize the material bandgap without altering ultrafast photophysics is reported. A new acceptor–donor–acceptor (A–D–A)-type small-molecule acceptor NCBDT is designed by modification of the D and A units of NFBDT. Compared to NFBDT, NCBDT exhibits upshifted highest occupied molecular orbital (HOMO) energy level mainly due to the additional octyl on the D unit and downshifted lowest unoccupied molecular orbital (LUMO) energy level due to the fluorination of A units. NCBDT has a low optical bandgap of 1.45 eV which extends the absorption range toward near-IR region, down to ≈ 860 nm. However, the 60 meV lowered LUMO level of NCBDT hardly changes the V_{oc} level, and the elevation of the NCBDT HOMO does not have a substantial influence on the photophysics of the materials. Thus, for both NCBDT- and NFBDT-based systems, an unusually slow (≈ 400 ps) but ultimately efficient charge generation mediated by interfacial charge-pair states is observed, followed by effective charge extraction. As a result, the PBDB-T:NCBDT devices demonstrate an impressive power conversion efficiency over 12%—among the best for solution-processed organic solar cells.

based on nonfullerene (NF) electron acceptors have made a great stride with power conversion efficiencies (PCEs) over 12%,^[3–6] which are comparable to or better than those of fullerene-based devices. These encouraging results may be partially ascribed to the rapid development of novel NF acceptors.^[7–14] Among various NF acceptors, nonfullerene small-molecule acceptors (NF-SMAs) with acceptor–donor–acceptor (A–D–A) structure have drawn tremendous interest because of their well-defined chemical structures and easily tuned energy levels.^[15–22] Zhan and co-workers reported some A–D–A-type NF-SMAs, such as (2,2'-[[6,6,12,12-tetrakis(4-hexylphenyl)-6,12-dihydrodithieno[2,3-d:2',3'-d']-s-indaceno[1,2-b:5,6-b']dithiophene-2,8-diyl]bis[methyldiyne(3-oxo-1H-indene-2,1(3H)-diylidene)])bis-propanedinitrile (ITIC) and (2,2'-[[4,4,9,9-tetrahexyl-4,9-dihydro-s-indaceno[1,2-b:5,6-b']dithiophene-2,7-diyl]bis[methyldiyne(3-oxo-1H-indene-2,1(3H)-diylidene)])bis-propanedinitrile (IDIC).^[23,24]

Organic solar cells (OSCs) have been regarded as one of the most promising technologies to utilize solar energy due to their solution processability, low cost, light weight, and flexibility.^[1,2] Recently, OSCs with bulk heterojunction architecture

High PCEs over 11% could be obtained in ITIC and derivative-based devices through donor mapping and device optimization.^[25–28] Such progress brings about a promising future for NF-based OSCs.

B. Kan, Dr. X. Wan, Dr. C. Li, X. Ke, Y. Wang, H. Feng, Y. Zhang, Dr. G. Long, Prof. Y. Chen
State Key Laboratory and Institute of Elemento-Organic Chemistry
The Centre of Nanoscale Science and Technology and Key Laboratory of Functional Polymer Materials
College of Chemistry
Nankai University
Tianjin 300071, China
E-mail: yschen99@nankai.edu.cn

J. Zhang, Dr. A. A. Bakulin
Department of Chemistry
Imperial College London
London SW7 2AZ, UK
E-mail: a.bakulin@imperial.ac.uk
J. Zhang, Prof. R. H. Friend
Cavendish Laboratory
University of Cambridge
JJ Thomson Avenue, Cambridge CB3 0HE, UK
Prof. F. Liu
Department of Physics and Astronomy
Shanghai Jiaotong University
Shanghai 200240, China

The ORCID identification number(s) for the author(s) of this article can be found under <https://doi.org/10.1002/adma.201704904>.

DOI: 10.1002/adma.201704904

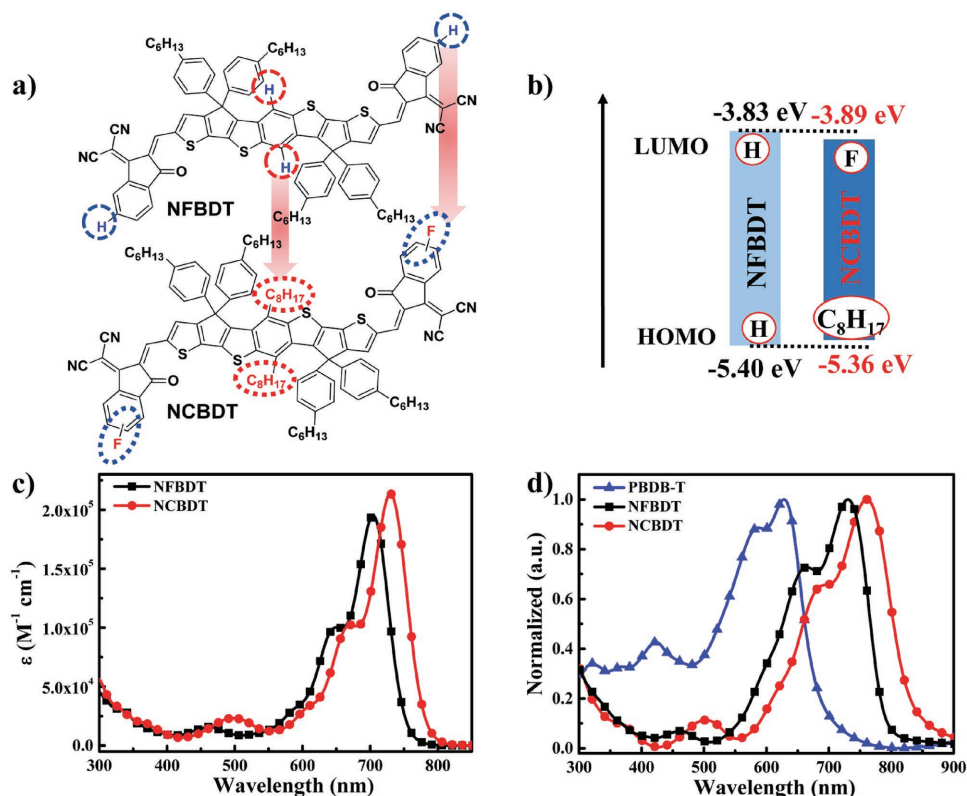


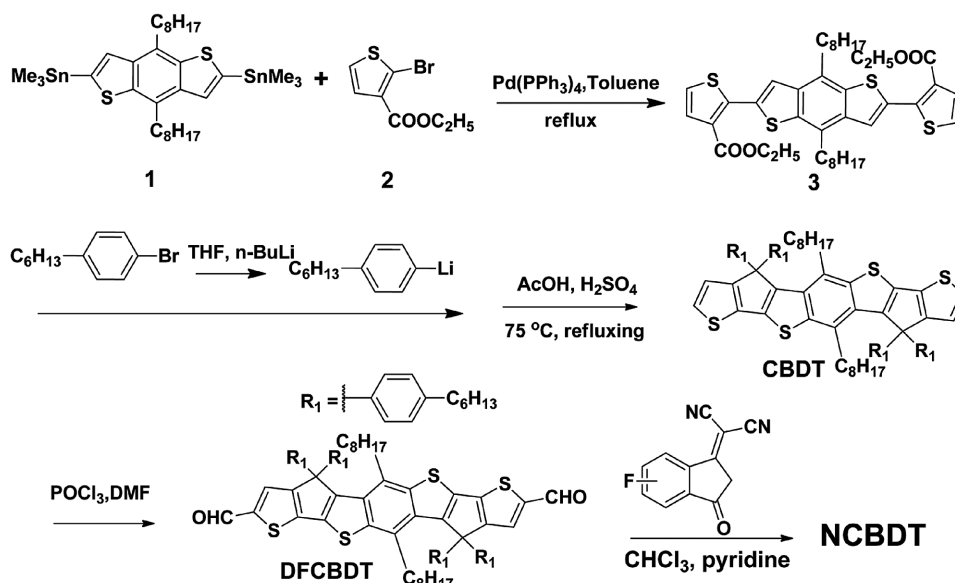
Figure 1. a) Chemical structures of NFBDT and NCBDT. b) The energy diagrams of NFBDT and NCBDT. c) Solution absorption spectra of NFBDT and NCBDT. d) Thin-film absorption spectra of NFBDT, NCBDT, and PBDB-T.

In our previous work, we have demonstrated that the energy levels of A–D–A-type small-molecule donors could be effectively tuned by adjusting the electron-donating ability of the D unit and the electron-withdrawing ability of the A unit.^[29] Given the reported results of A–D–A-type NF-SMAs,^[10,30] these rather successful strategies from A–D–A donors could also be applied to the design of NF-SMAs with versatile energy levels. Recently, we have developed an A–D–A-type NF-SMA, namely NFBDT, using heptylcyclopentadithiophene as the core unit (D) and 2-(2,3-dihydro-3-oxo-1H-inden-1-ylidene)propanedinitrile (INCN) as the end groups (A). By combining with a wide bandgap polymer donor material PBDB-T (poly[(2,6-(4,8-bis(5-(2-ethylhexyl)thiophen-2-yl)-benzo[1,2-b:4,5-b']dithiophene))-alt-(5,5-(1',3'-di-2-thienyl-5',7'-bis(2-ethylhexyl)benzo[1',2'-c:4',5'-c']dithiophene-4,8-dione))]), the device exhibited PCE over 10% due to its complementary absorption range and balanced charge transport abilities.^[31] Modifying the D and A unit of NFBDT allows the energy levels to be fine-tuned, opening the possibility of a low-bandgap NF-SMA. This might be an effective approach to extend its absorption range, which would be beneficial for achieving higher short-circuit current density (J_{sc}).

In this contribution, through molecular modifications of NFBDT, we designed and synthesized a new low-bandgap A–D–A-type NF-SMA (namely NCBDT) as shown in **Figure 1a**. For the INCN end unit, a strong electron-withdrawing fluorine atom (F) was introduced to shift down the highest occupied molecular orbital (HOMO) and lowest unoccupied molecular orbital (LUMO) energy levels.^[4,6,27,32] In its fused-ring core,

a weak electron-donating alkyl group (octyl) was introduced to 4,8-positions of the central benzo[1,2-b:4,5-b']dithiophene (BDT) unit to increase the HOMO energy level.^[33,34] In contrast to many polymer:fullerene systems,^[35] the reduction of energetic offsets between the molecular HOMO orbitals does not have a substantial influence on the photophysics of the material. Both NCBDT- and NFBDT-based systems thus show slow (≈ 400 ps) but ultimately efficient free charge generation mediated by interfacial charge-pair (ICP) states (discussed below). Thus, the lower driving energy does not have a detrimental effect on charge generation, opening the way for the optimization of current and voltage losses simultaneously. Such delicate structural modifications overall decrease the optical bandgap (E_g^{opt}) of NCBDT to 1.45 eV which extends light harvesting of PBDB-T:NCBDT to near-IR region and boosts the J_{sc} to an outstanding value of >20 mA cm⁻², but maintains the relatively high open-circuit voltage (V_{oc}) with a smaller V_{oc} loss. Thus, in combination with a V_{oc} of 0.839 V and high fill factor (FF) of 71%, such high J_{sc} allows the optimized PBDB-T:NCBDT device to reach a remarkable PCE over 12%—one of the best performances for photovoltaic devices with such a low-bandgap NF-SMA.

The target molecule NCBDT was synthesized via a five-step chemical reaction sequence as illustrated in **Scheme 1**, and the detailed synthetic procedures including characterization data are presented in the Supporting Information. Stille coupling reaction of commercial compounds 1 and 2 produced compound 3. The key fused-ring compound



Scheme 1. Synthetic route of NCBDT.

(4,4,10,10-tetrakis(4-hexylphenyl)-4,10-dihydro-5,11-dioctylthieno[3',2':4,5]cyclopenta[1,2-b]thieno[2'',3'':3',4']cyclopenta[1',2':4,5]thieno[2,3-f][1]benzothiophene) (CBDT) was synthesized via a nucleophilic reaction and the acid-mediated Friedel–Crafts reaction with overall yield >60%. The dialdehyde compound (4,4,10,10-tetrakis(4-hexylphenyl)-4,10-dihydro-5,11-dioctylthieno[3',2':4,5]cyclopenta[1,2-b]thieno[2'',3'':3',4']cyclopenta[1',2':4,5]thieno[2,3-f][1]benzothiophene-2,8-dicarboxaldehyde) (DFCBDT) was prepared by the Vilsmeier–Haack reaction using POCl₃ and DMF, and its chemical structure was fully characterized by ¹H/¹³C NMR and mass spectrum. NCBDT was obtained as a dark-blue solid by the Knoevenagel condensation of DFCBDT with F-INCN. Though NCBDT is a mixture due to the two isomers of F-INCN, consistent performance was observed between multiple batches. NCBDT shows excellent solubility in chloroform, chlorobenzene, and other common organic solvents due to six side chains. The thermal stability of NCBDT was evaluated by thermogravimetric analysis (Figure S1a, Supporting Information) under nitrogen atmosphere. The molecule did not decompose until 330 °C, which is adequate for future application. No melting point or crystallization point was found from its differential scanning calorimetry curve as shown in Figure S1b (Supporting Information).

The solution absorption spectra of NFBDT and NCBDT are presented in Figure 1c, and their thin-film absorption spectra together with that of PBDB-T are shown in Figure 1d. In comparison to NFBDT, NCBDT in dilute chloroform solution exhibits an obvious redshifted absorption peak at 730 nm as well as a higher maximum extinction coefficient of $2.1 \times 10^5 \text{ M}^{-1} \text{ cm}^{-1}$. From Figure 1d, NCBDT film displays an absorption peak located at 760 nm, which is redshifted by nearly 30 nm compared to that of NFBDT. The $E_{\text{g}}^{\text{opt}}$ of NCBDT (1.45 eV), calculated from its thin-film absorption onset at 853 nm, is 0.11 eV smaller than NFBDT. The combination of the donor PBDB-T with NCBDT extends the absorption range to ≈860 nm.

The energy levels of NCBDT were investigated by cyclic voltammetry (CV; as shown in Figure S2 in the Supporting Information) under the identical conditions used for NFBDT. The HOMO level for NCBDT was estimated to be −5.36 eV, which is 0.04 eV higher than that of NFBDT (−5.40 eV), probably due to the introduction of octyl side chain on the central D unit. The LUMO level for NCBDT was measured to be −3.89 eV, lower than −3.83 eV for NFBDT, due to the introduction of F atom on the ending INCN unit. The energy levels obtained from CV measurement are consistent with the calculated values using density functional theory at the B3LYP/6-31G* level (Table S1, Supporting Information). These results indicate that this molecular design strategy indeed narrows the bandgap of NFBDT, in good agreement with measured optical bandgaps. To investigate the exciton dissociation behavior in the PBDB-T:NCBDT optimized blend films, photoluminescence (PL) quenching experiments were performed at the excitation wavelength of 600 nm for PBDB-T donor and 700 nm for NCBDT acceptor. Figure S4 (Supporting Information) shows that the PL quenching efficiencies for PBDB-T and NCBDT are 98.7% and 96.5%, respectively, indicating highly efficient exciton dissociation at heterojunction interface.

Solution-processed OSC devices were fabricated using a normal structure of ITO/PEDOT:PSS/PBDB-T:NCBDT/PDINO/Al, where PDINO (perylene diimide functionalized with amino N-oxide)^[36] was selected as electron transport layer (Table S5, Supporting Information). After systematic device optimization (Tables S2–S5, Supporting Information), the ratio of PBDB-T:NCBDT (1:0.8) and the thickness of the active layer (≈100 nm) were found to be similar to those for PBDB-T:NFBDT. The optimal performance for PBDB-T:NCBDT devices was obtained via solvent vapor annealing treatment (Table S3, Supporting Information). The corresponding current-density–voltage (*J*–*V*) curve of the optimal device based on NCBDT is shown as Figure 2a, and their best photovoltaic parameters together with those of NFBDT are summarized in

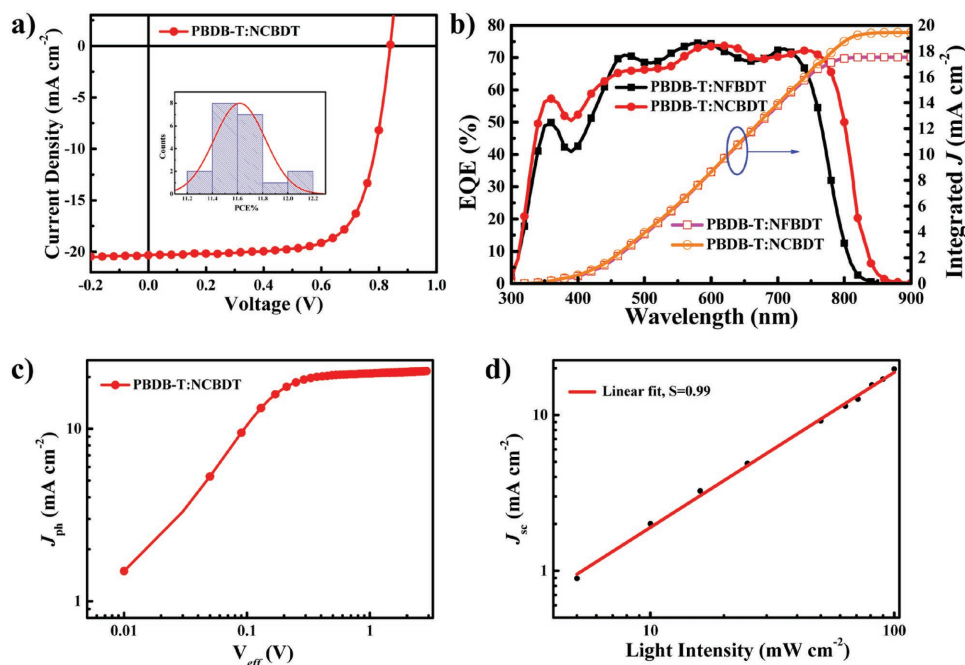


Figure 2. a) Optimal current density–voltage (J – V) curve of the device based on PBDB-T:NCBDT under the illumination of AM 1.5G (100 mW cm^{-2}). b) EQE spectra and the corresponding integrated J curves of devices based on PBDB-T:NFBDT and PBDB-T:NCBDT, respectively. c) J_{ph} versus V_{eff} and (d) Light-intensity dependence of J_{sc} of NCBDT-based devices.

Table 1. Compared with PBDB-T:NFBDT-based devices, PBDB-T:NCBDT-based devices achieved an enhanced J_{sc} of 20.33 mA cm^{-2} , better fill factor of 71.0%, and improved PCE of 12.12%. The energy loss ($E_{\text{loss}} = E_{\text{g}}^{\text{opt}} - eV_{\text{oc}}$) for the PBDB-T:NCBDT-based device is merely 0.61 eV, lower than 0.69 eV energy loss for the PBDB-T:NFBDT-based device, and thus a moderate and hardly changed V_{oc} around 0.84 V could be obtained. These results indicate that it is possible to achieve a delicate and difficult balance between the J_{sc} and V_{oc} in this case, when the J_{sc} is significantly improved by narrowing the acceptor bandgap, while V_{oc} is maintained at almost the same level. As far as we know, this encouraging PCE over 12% with a high J_{sc} over 20 mA cm^{-2} is one of the best results for low-bandgap NF-SMA-based devices with E_{loss} around 0.60 eV.

The external quantum efficiency (EQE) was measured to verify the higher J_{sc} value for NCBDT-based device. As shown in Figure 2b, the NCBDT-based device reached a maximum EQE value of 74% and over 70% across the range of 550–770 nm. Note that the NCBDT-based device displayed $\approx 35 \text{ nm}$ redshifted photocurrent responses compared to the NFBDT-based device, which is in agreement with the trend of absorption profiles for their corresponding blend films (Figure S5, Supporting Information). The integrated J curve for NCBDT-based device, along with the EQE curve (Figure 2b), is almost the same as that

of NFBDT until 750 nm, but becomes higher in the range of 750–850 nm which is ascribed to the contribution of NCBDT acceptor. The integrated current densities between 750 and 850 nm for the NFBDT and NCBDT devices are 1.31 and 2.93 mA cm^{-2} , respectively. The difference between these two values is quite similar to the difference of the overall currents of their corresponding devices, which strongly indicates that the improved current is mainly due to the new acceptor NCBDT absorption in this region. Importantly, compared to the PBDB-T:NFBDT device, efficient hole transfer process from NCBDT to PBDB-T even with a smaller HOMO energy offset could also be realized, which is supported by the high EQE values in the range of 700–800 nm and PL results.

In order to investigate the charge generation and charge recombination behavior in the NCBDT-based optimal devices, the photocurrent (J_{ph}) versus the effective applied voltage (V_{eff}) and the light-intensity dependence of J_{sc} were measured according to the reported methods.^[37,38] Figure 2c shows that J_{ph} becomes saturated (J_{sat}) when V_{eff} exceeds 1.6 V, indicating high charge extraction probability at higher voltages. The free charge extraction of the NCBDT-based device estimated from the ratio of $J_{\text{ph}}/J_{\text{sat}}$ is higher than that of NFBDT-based device under the short circuit (97% for NCBDT vs 94% for NFBDT) and maximal power output conditions (84% for NCBDT vs 81%

Table 1. Optimal device parameters of the NFBDT-based and NCBDT-based devices under the illumination of AM 1.5G (100 mW cm^{-2}).

BHJ layer	V_{oc} [V]	J_{sc} [mA cm^{-2}]	FF [%]	PCE ^{a)} [%]	E_{loss} ^{b)} [eV]
PBDB-T:NFBDT ^{c)}	0.863 ± 0.004 (0.868)	17.35 ± 0.27 (17.85)	66.3 ± 0.4 (67.2)	10.15 ± 0.17 (10.42)	0.69
PBDB-T:NCBDT	0.835 ± 0.003 (0.839)	19.73 ± 0.45 (20.33)	70.2 ± 0.5 (71.0)	11.62 ± 0.21 (12.12)	0.61

^{a)}The average PCE was obtained from 20 devices, and the best results are provided in parentheses; ^{b)} $E_{\text{loss}} = E_{\text{g}}^{\text{opt}} - eV_{\text{oc}}$; ^{c)}Cited from ref. [31].

for NFBDT). From the light-intensity dependence of J_{sc} results (Figure 2d), a slope of 0.99 is obtained for the NCBDT-based device, which is steeper than the slope of 0.95 for the NFBDT-based device. This implies even lower (minimal) bimolecular recombination in the NCBDT-based optimal device. The electron mobility of NCBDT in pristine thin film measured by space-charge-limited current (SCLC) measurement (Figure S6, Supporting Information) is $1.95 \times 10^{-4} \text{ cm}^{-2} \text{ V}^{-1} \text{ s}^{-1}$, larger than that of NFBDT ($1.52 \times 10^{-4} \text{ cm}^{-2} \text{ V}^{-1} \text{ s}^{-1}$) and correlating with their morphology discussed below. In addition, the electron and hole mobilities for PBDB-T:NCBDT blend films were estimated to be 1.58×10^{-4} and $3.92 \times 10^{-4} \text{ cm}^{-2} \text{ V}^{-1} \text{ s}^{-1}$, respectively, which are higher than those of PBDB-T:NFBDT blend films. For the SCLC testing, the thickness for their pristine films and blend films are controlled to be 100 nm.

Summarizing the steady-state results, we conclude that the enhanced charge generation and higher/more balanced transport of the NCBDT-based device lead to about $\approx 4\%$ improvement in FF compared to the NFBDT-based solar cell. Meanwhile, the redshifted absorption of NCBDT in the near-IR region provides an extra $\approx 13\%$ boost in the current output at the expense of a much smaller $\approx 3\%$ loss in V_{oc} . The combination of all these factors makes the NCBDT-based device about 14% more efficient than the NFBDT-based device, allowing the NCBDT-based device to reach $>12\%$ efficiency.

The morphologies of the PBDB-T:NCBDT blend layer were studied by tapping-mode atomic force microscopy (AFM) and transmission electron microscopy (TEM). As observed from the AFM image (Figure 3a), the surface of the PBDB-T:NCBDT film is quite uniform and smooth with a small root-mean-square surface roughness value of 1.27 nm. From TEM image (Figure 3b), phase separation with proper domain size could be observed for the PBDB-T:NCBDT film. 2D grazing-incidence wide-angle X-ray scattering (2D-GIXD) method was used to investigate the microstructural differences between pure NFBDT and NCBDT films shown in Figure S7a,b (Supporting Information). In-plane and out-of-plane line-cut profiles are presented as Figure S7c,d, respectively, in the Supporting Information. The newly designed NCBDT molecule prefers a face-on molecular orientation, supported by its (100) diffraction peak along the q_{xy} direction and a sharp (010) diffraction peak of π - π stacking along the q_z direction, which is quite similar to NFBDT. The (100) peak for NCBDT is located at 0.30 \AA^{-1} , corresponding to the interchain distance of 20.9 \AA for NCBDT in the in-plane direction. The larger interchain distance for NCBDT compared with that of NFBDT could be attributed to the additional octyl attached to the central BDT block. However, the π - π stacking distance for NCBDT is 3.43 \AA , smaller than 3.47 \AA for NFBDT. Estimated by Scherrer equation,^[39] these correspond to the crystal coherence length (CCL) in the (010) direction of

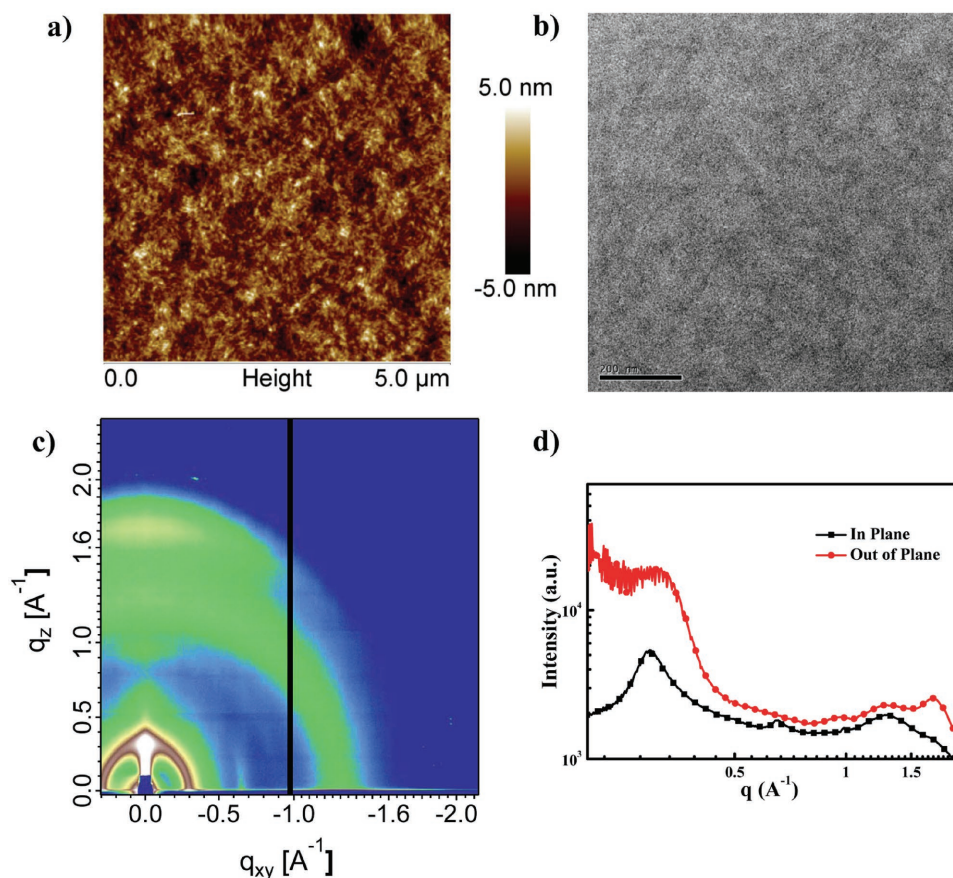


Figure 3. a) AFM and b) TEM images of the PBDB-T:NCBDT blend film, and the scale bar is 200 nm. c) 2D-GIXD pattern of the PBDB-T:NCBDT blend. d) In-plane and out-of-plane line cuts of the GIXD pattern.

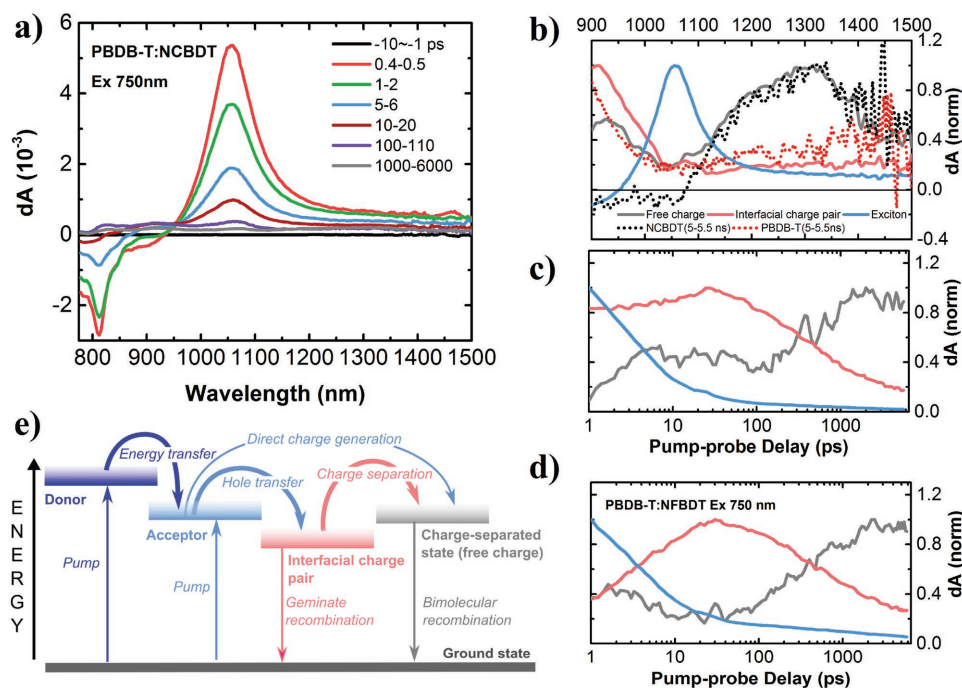


Figure 4. Transient absorption spectroscopy of PBDB-T:NCBDT and PBDB-T:NFBDT with excitation at 750 nm. a) Transient spectra of the PBDB-T:NCBDT blend at different delay times. b,c) The spectral components and relevant kinetics extracted from TA data for PBDB-T:NCBDT using the global analysis. d) Kinetics extracted from TA data for PBDB-T:NFBDT. e) State energy diagram showing the relevant photophysical processes.

49.5 Å for NCBDT and 38.8 Å for NFBDT. The smaller π - π stacking distance and the increased CCL in the (010) direction of NCBDT, in combination with its face-on molecular orientation, are more favorable for charge transport as evidenced by its higher electron mobilities.^[40,41] As seen from the 2D-GIXD pattern for the PBDB-T:NCBDT blend film and its corresponding in-plane/out-of-plane line cuts (Figure 3c,d), the alkyl to alkyl (100) and π - π stacking (010) regions both exhibit merged diffraction signals from PBDB-T donor and NCBDT acceptor. It is rather hard to obtain quantitative analysis from the GIXD results. In the PBDB-T:NCBDT blend film, both compounds adopt a preferred face-on orientation, inferred from the combined (010) peaks in the out-of-plane direction, which is the same as that of the PBDB-T:NFBDT film. These results indicate that the blend of these two acceptors with the same donor PBDB-T adopt rather similar morphology.

To specifically address the molecular-scale charge generation and recombination properties, we perform an ultrafast spectroscopic study on both photovoltaic systems. **Figure 4** presents the results of ultrafast transient absorption (TA) experiments after photoexcitation of the studied materials with 750 nm light. Excitation at this wavelength matches the absorption band of the acceptors, and therefore should lead to charge generation through a hole transfer process. To avoid the complicated influences of ground-state bleach as well as thermal and electroabsorption contributions to the response, we analyzed the spectra in the >900 nm region where only the photoinduced absorption (PIA) features of charges and excitons are present. Global analysis of the multidimensional spectroscopic data shows that three types of species contribute to the PIA signals. For PBDB-T:NCBDT, the decomposed spectral signatures of these species

are shown in Figure 4b and the corresponding dynamics of these species are presented in Figure 4c (video in the Supporting Information). The first species (blue curve, Figure 4b,c) is assigned to excitons as the spectral response matches that of pure NCBDT (Figure S9, Supporting Information). The second species (Figure 4b,c, gray solid line) is assigned to free charges in PBDB-T and NCBDT, as their spectral shapes also match the long-lived spectra from the pure materials (dashed lines). The third species (red lines) exhibits spectral signatures that are different from those observed in the pure materials and also shows complex temporal behavior. Their population of this species first grows until ≈ 30 ps, which is on the same timescale as the exciton decay (blue line). The population then decays steadily with an ≈ 400 ps time constant, as the population of charges increases. All these indicate that the third species is an intermediate between excitons and free charge generation, and as such can be assigned to charge pairs residing at the donor-acceptor interface or triplet excitons.^[42,43] However, light-fluence-dependent measurement (Figure S10, Supporting Information) reveals that the relative number of intermediate states, as well as the relative number of second species, decreases with increasing illumination intensity. This indicates that neither intermediate nor final states can be triplets (triplet generation is a bimolecular process). Most likely, intermediate states have polaron character and are related to the charges residing in the donor-acceptor mixed phase. We note that though interfacial charge pairs are in a sense similar to widely discussed charge-transfer excitons, we avoid to use this notation as we cannot quantify the level of interaction between the electron and the hole. The characteristic spectral signatures of interfacial charge pairs, dissimilar from those of free

carriers, may be the result of specific structural conformations of the molecules not well packed in pure material domains. Additional minor contribution may come from donor–acceptor electronic couplings. Fluence-dependent kinetics also allow to attribute the minor decays of free carrier between 10 and 100 ps and after 2 ns to bimolecular recombination. These processes are prominent at very high photoexcitation density and can be detected in TA, but should not play an important role at solar illumination conditions. The results of PBDB-T:NFBDT blend (Figure 4d; Figure S11, Supporting Information) appeared to be qualitatively very similar to PBDB-T:NCBDT consistent with the morphology discussed above, which means the photophysics of both materials can be described using the same model. When sample is excited at wavelength <620 nm, PBDB-T excitation leads to an ultrafast energy transfer to acceptor within 1 ps, followed by hole-transfer charge dynamics identical to those described above (more details are provided in the Supporting Information).

Figure 4e outlines the general model of the photophysical processes described above. Acceptor excitation due to the light absorption, or due to the energy transfer from donor, leads to the (i) direct free charge generation or (ii) formation of ICPs. We estimate that around two-thirds of free carriers come from the separation of ICPs and another one-third from the direct generation. One possible reason for this can be that $\approx 35\%$ efficient generation of free charges is happening through the “hot”^[44,45] or delocalized^[46] charge-transfer states, while the rest of photocurrent is generated through the “cold” ICP intermediates. Another possibility is that different local morphologies lead to the different charge generation pathways, direct or ICP mediated. Based on the existing data, we cannot differentiate between these two different mechanisms. The timescale of conversion from ICPs to free charges is estimated to be around 400 ps, which is in striking contrast to sub-ps free carrier formation observed in most polymer–fullerene blends^[47–50] and some other NF materials.^[12,19,51] This highlights the conceptually different molecular mechanism of charge generation in high-performance NF acceptors such as NFBDT and NCBDT. Interestingly, the photophysics for both studied materials are very similar despite the HOMO–HOMO offset in NCBDT-based blend is smaller by ≈ 40 meV. This indicates that the charge generation in the studied class of donor–acceptor systems is not very sensitive to the driving energy for charge separation, allowing further optimizations of acceptor bandgaps and V_{oc} . Delicate control of band offsets via energy level optimization might be a powerful approach to design optimal combinations of acceptor and donor materials, to increase solar light absorption (for higher J_{sc}) while minimizing the loss of V_{oc} .

In conclusion, we designed and synthesized a new A–D–A-type acceptor NCBDT by the simultaneous introduction of octyl on the D unit and fluorine atoms on the A unit of the molecule NFBDT. Compared to NFBDT, NCBDT exhibits higher electron mobility and a smaller optical bandgap of 1.45 eV resulting in redshifted absorption range and a significant increase in the device photocurrent. But the lowered acceptor’s LUMO level of NCBDT hardly changes the V_{oc} partially due to a lower energy loss down to the remarkable 0.61 eV per photon. Also, significantly, the elevation of the HOMO level (smaller offset) does not have a substantial influence on the photophysics of

the materials. But, in striking contrast to polymer–fullerene materials, for both NCBDT- and NFBDT-based systems, a slow (≈ 400 ps) but ultimately efficient charge generation mediated by interfacial charge-pair states was observed. This is followed by effective charge extraction and low bimolecular recombination. As a result, the device based on PBDB-T:NCBDT offers an outstanding PCE of 12.12% with a high J_{sc} over 20 mA cm⁻², which is one of the highest recorded performances among OSC devices with low-bandgap acceptors. Our results demonstrate that NF-SMAs with high performance could be obtained by fine-tuning the energy levels through delicate chemical structure modification. Considering the versatility of BDT derivatives and the apparent insensitivity of the photophysics to the reduction of the band offsets, we expect that low energy loss close to 0.50 eV is achievable by employing similar strategies involving the fine-tuning of molecular energy levels and bandgaps, resulting in solar cells with superior efficiencies.

Supporting Information

Supporting Information is available from the Wiley Online Library or from the author.

Acknowledgements

B.K. and J.Z. contributed equally to this work. The authors gratefully acknowledge the financial support from MoST (Grant Nos. 2014CB643502 and 2016YFA0200200), NSFC (Grant Nos. 21421001, 91633301, 51773095, and 17CZDJC31100) of China, 111 Project (Grant No. B12015). The authors thank Tom Hopper for proofreading and his comments on the manuscript. J.Z. thanks the China Scholarship Council for a Ph.D. scholarship. A.A.B. is a Royal Society Research University Research Fellow. The morphological characterization of the active layers was supported by the DOE-Funded Energy Frontier Research Center on Polymer-Based Materials for Harvesting Solar Energy (DE-SC0001087). Portions of this research were carried out at the Advanced Light Source, Berkeley National Laboratory, which was supported by the DOE, Office of Science, and Office of Basic Energy Sciences.

Conflict of Interest

The authors declare no conflict of interest.

Keywords

charge separation, high-performance organic solar cells, low bandgap, small-molecule nonfullerene acceptors

Received: August 27, 2017

Revised: October 23, 2017

Published online:

- [1] R. F. Service, *Science* **2011**, 332, 293.
- [2] G. Li, R. Zhu, Y. Yang, *Nat. Photonics* **2012**, 6, 153.
- [3] S. Li, L. Ye, W. Zhao, S. Zhang, S. Mukherjee, H. Ade, J. Hou, *Adv. Mater.* **2016**, 28, 9423.
- [4] F. Zhao, S. Dai, Y. Wu, Q. Zhang, J. Wang, L. Jiang, Q. Ling, Z. Wei, W. Ma, W. You, C. Wang, X. Zhan, *Adv. Mater.* **2017**, 29, 1700144.

- [5] W. Zhao, S. Li, S. Zhang, X. Liu, J. Hou, *Adv. Mater.* **2017**, *29*, 1604059.
- [6] W. Zhao, S. Li, H. Yao, S. Zhang, Y. Zhang, B. Yang, J. Hou, *J. Am. Chem. Soc.* **2017**, *139*, 7148.
- [7] Y. Lin, X. Zhan, *Mater. Horiz.* **2014**, *1*, 470.
- [8] C. B. Nielsen, S. Holliday, H. Y. Chen, S. J. Cryer, I. McCulloch, *Acc. Chem. Res.* **2015**, *48*, 2803.
- [9] C. Zhan, J. Yao, *Chem. Mater.* **2016**, *28*, 1948.
- [10] N. Liang, W. Jiang, J. Hou, Z. Wang, *Mater. Chem. Front.* **2017**, *1*, 1291.
- [11] D. Baran, R. S. Ashraf, D. A. Hanifi, M. Abdelsamie, N. Gasparini, J. A. Rohr, S. Holliday, A. Wadsworth, S. Lockett, M. Neophytou, C. J. M. Emmott, J. Nelson, C. J. Brabec, A. Amassian, A. Salleo, T. Kirchartz, J. R. Durrant, I. McCulloch, *Nat. Mater.* **2017**, *16*, 363.
- [12] J. Liu, S. Chen, D. Qian, B. Gautam, G. Yang, J. Zhao, J. Bergqvist, F. Zhang, W. Ma, H. Ade, O. Inganäs, K. Gundogdu, F. Gao, H. Yan, *Nat. Energy* **2016**, *1*, 16089.
- [13] A. Tang, C. Zhan, J. Yao, E. Zhou, *Adv. Mater.* **2017**, *29*, 1600013.
- [14] Q. Wu, D. Zhao, A. M. Schneider, W. Chen, L. Yu, *J. Am. Chem. Soc.* **2016**, *138*, 7248.
- [15] Y. Lin, Z.-G. Zhang, H. Bai, J. Wang, Y. Yao, Y. Li, D. Zhu, X. Zhan, *Energy Environ. Sci.* **2015**, *8*, 610.
- [16] N. Qiu, H. Zhang, X. Wan, C. Li, X. Ke, H. Feng, B. Kan, H. Zhang, Q. Zhang, Y. Lu, Y. Chen, *Adv. Mater.* **2017**, *29*, 1604964.
- [17] V. Gupta, A. Bagui, S. P. Singh, *Adv. Funct. Mater.* **2017**, *27*, 1603820.
- [18] W. Zhao, S. Zhang, J. Hou, *Sci. China Chem.* **2016**, *59*, 1574.
- [19] H. Bin, L. Gao, Z.-G. Zhang, Y. Yang, Y. Zhang, C. Zhang, S. Chen, L. Xue, C. Yang, M. Xiao, Y. Li, *Nat. Commun.* **2016**, *7*, 13651.
- [20] Y. Liu, H. Zhang, Y. Sun, X. Wan, Y. Chen, *Sci. China Mater.* **2017**, *60*, 49.
- [21] H. Zhang, Y. Liu, Y. Sun, M. Li, W. Ni, Q. Zhang, X. Wan, Y. Chen, *Sci. China Chem.* **2017**, *60*, 366.
- [22] F. Liu, Z. Zhou, C. Zhang, T. Vergote, H. Fan, F. Liu, X. Zhu, *J. Am. Chem. Soc.* **2016**, *138*, 15523.
- [23] Y. Lin, J. Wang, Z. G. Zhang, H. Bai, Y. Li, D. Zhu, X. Zhan, *Adv. Mater.* **2015**, *27*, 1170.
- [24] Y. Lin, Q. He, F. Zhao, L. Huo, J. Mai, X. Lu, C.-J. Su, T. Li, J. Wang, J. Zhu, Y. Sun, C. Wang, X. Zhan, *J. Am. Chem. Soc.* **2016**, *138*, 2973.
- [25] Y. Yang, Z.-G. Zhang, H. Bin, S. Chen, L. Gao, L. Xue, C. Yang, Y. Li, *J. Am. Chem. Soc.* **2016**, *138*, 15011.
- [26] Y. Lin, F. Zhao, Y. Wu, K. Chen, Y. Xia, G. Li, S. K. K. Prasad, J. Zhu, L. Huo, H. Bin, Z.-G. Zhang, X. Guo, M. Zhang, Y. Sun, F. Gao, Z. Wei, W. Ma, C. Wang, J. Hodgkiss, Z. Bo, O. Inganäs, Y. Li, X. Zhan, *Adv. Mater.* **2017**, *29*, 1604155.
- [27] S. Dai, F. Zhao, Q. Zhang, T.-K. Lau, T. Li, K. Liu, Q. Ling, C. Wang, X. Lu, W. You, X. Zhan, *J. Am. Chem. Soc.* **2017**, *139*, 1336.
- [28] S. Chen, H. J. Cho, J. Lee, Y. Yang, Z.-G. Zhang, Y. Li, C. Yang, *Adv. Energy Mater.* **2017**, 1701125.
- [29] Y. Chen, X. Wan, G. Long, *Acc. Chem. Res.* **2013**, *46*, 2645.
- [30] Y. Lin, X. Zhan, *Acc. Chem. Res.* **2016**, *49*, 175.
- [31] B. Kan, H. Feng, X. Wan, F. Liu, X. Ke, Y. Wang, Y. Wang, H. Zhang, C. Li, J. Hou, Y. Chen, *J. Am. Chem. Soc.* **2017**, *139*, 4929.
- [32] H. Yao, Y. Cui, R. Yu, B. Gao, H. Zhang, J. Hou, *Angew. Chem., Int. Ed.* **2017**, *56*, 3045.
- [33] J. Mei, Z. Bao, *Chem. Mater.* **2014**, *26*, 604.
- [34] J. Kim, A. Han, J. Seo, J. Oh, C. Yang, *Chem. Mater.* **2012**, *24*, 3464.
- [35] S. Dimitrov, J. Durrant, *Chem. Mater.* **2014**, *26*, 616.
- [36] Z.-G. Zhang, B. Qi, Z. Jin, D. Chi, Z. Qi, Y. Li, J. Wang, *Energy Environ. Sci.* **2014**, *7*, 1966.
- [37] P. W. Blom, V. D. Mihailetschi, L. J. A. Koster, D. E. Markov, *Adv. Mater.* **2007**, *19*, 1551.
- [38] C. M. Proctor, M. Kuik, T.-Q. Nguyen, *Prog. Polym. Sci.* **2013**, *38*, 1941.
- [39] D.-M. Smilgies, *J. Appl. Crystallogr.* **2009**, *42*, 1030.
- [40] J. Rivnay, S. C. Mannsfeld, C. E. Miller, A. Salleo, M. F. Toney, *Chem. Rev.* **2012**, *112*, 5488.
- [41] F. Liu, Y. Gu, X. Shen, S. Ferdous, H.-W. Wang, T. P. Russell, *Prog. Polym. Sci.* **2013**, *38*, 1990.
- [42] A. Rao, P. C. Y. Chow, S. Gelinias, C. W. Schlenker, C.-Z. Li, H.-L. Yip, A. K. Y. Jen, D. S. Ginger, R. H. Friend, *Nature* **2013**, *500*, 435.
- [43] S. M. Menke, A. Sadhanala, M. Nikolka, N. A. Ran, M. K. Ravva, S. Abdel-Azeim, H. L. Stern, M. Wang, H. Sirringhaus, T.-Q. Nguyen, J.-L. Brédas, G. C. Bazan, R. H. Friend, *ACS Nano* **2016**, *10*, 10736.
- [44] G. Grancini, M. Maiuri, D. Fazzi, A. Petrozza, H.-J. Egelhaaf, D. Brida, G. Cerullo, G. Lanzani, *Nat. Mater.* **2013**, *12*, 29.
- [45] A. E. Jailaubekov, A. P. Willard, J. R. Tritsch, W.-L. Chan, N. Sai, R. Gearba, L. G. Kaake, K. J. Williams, K. Leung, P. J. Rossky, X.-Y. Zhu, *Nat. Mater.* **2013**, *12*, 66.
- [46] A. A. Bakulin, A. Rao, V. G. Pavelyev, P. H. M. van Loosdrecht, M. S. Pshenichnikov, D. Niedzialek, J. Cornil, D. Beljonne, R. H. Friend, *Science* **2012**, *335*, 1340.
- [47] S. Gelinias, A. Rao, A. Kumar, S. L. Smith, A. W. Chin, J. Clark, T. S. van der Poll, G. C. Bazan, R. H. Friend, *Science* **2014**, *343*, 512.
- [48] A. C. Jakowetz, M. L. Böhm, A. Sadhanala, S. Huettner, A. Rao, R. H. Friend, *Nat. Mater.* **2017**, *16*, 551.
- [49] J. De Jonghe-Risse, M. Scarongella, J. C. Brauer, E. Buchaca-Domingo, J.-E. Moser, N. Stingelin, N. Banerji, *Nat. Commun.* **2016**, *7*, 12556.
- [50] F. Provencher, N. Bérubé, A. W. Parker, G. M. Greetham, M. Towrie, C. Hellmann, M. Côté, N. Stingelin, C. Silva, S. C. Hayes, *Nat. Commun.* **2014**, *5*, 4288.
- [51] D. Baran, T. Kirchartz, S. Wheeler, S. Dimitrov, M. Abdelsamie, J. Gorman, R. S. Ashraf, S. Holliday, A. Wadsworth, N. Gasparini, P. Kaienburg, H. Yan, A. Amassian, C. J. Brabec, J. R. Durrant, I. McCulloch, *Energy Environ. Sci.* **2016**, *9*, 3783.